Quantum many-body scars in transverse field Ising ladders and beyond

Van Voorden, B.; Minář, J.; Schoutens, K.

Quantum many-body scars in transverse field Ising ladders and beyond

Bart van Voorden [©],[*] Jiří Minář [©],[†] and Kareljan Schoutens [©][‡]

Institute for Theoretical Physics, University of Amsterdam, Science Park 904, 1098 XH Amsterdam, the Netherlands

We identify quantum many-body scars in the transverse field quantum Ising model on a ladder. We make explicit how the corresponding (mid spectrum, low entanglement) many-body eigenstates can be approximated by injecting quasiparticle excitations into an exact, zero-energy eigenstate, which is of valence bond solid type. Next, we present a systematic construction of product states characterized, in the limit of a weak transverse field, by a sharply peaked local density of states. We describe how the construction of these 'peak states' generalizes to arbitrary dimension and we show that on the ladder their number scales with system size as the square of the golden ratio.

Introduction. Understanding of nonequilibrium dynamics and thermalization is at the forefront of research on quantum many-body systems. These developments led to the formulation of the eigenstate thermalization hypothesis (ETH) [1–3], predicting fast thermalization following a quench from a generic many-body state. A number of exceptions to this behavior have been identified, namely integrable [4,5] and many-body localized systems [6–12], which both preclude thermalization due to a number of conserved charges. A recent observation of nonthermalizing behavior in a chain of Rydberg atoms [13] described by a so-called PXP Hamiltonian [14], has been interpreted in terms of quantum many-body scars (QMBS) [15,16]. QMBS are an example of weak ETH breaking, i.e., lack of thermalization for a limited set of initial states. This observation led to a number of works including further studies on the PXP-model [17–25], constrained [26–29] and topological [30] Hamiltonians, the role of integrability [31], quantum chaos [32–38], and fragmentation of Hilbert space [39–42]. Simultaneously, QMBS have been described in a range of models, including the AKLT model [43–47], spin chains [48–51] and arrays [52], boson [53] and spin-boson [54,55], and driven systems [56–62].

Interestingly and to the best of our knowledge, the paradigmatic model of quantum magnetism, the quantum Ising model, has not been analyzed from the perspective of QMBS beyond a chain [25,36]. Here we note that nonthermal behavior following a quench has been investigated in the longitudinal field Ising model [63,64] and in the Ising model with long range interactions [65], where the absence of thermalization was interpreted in terms of meson quasiparticles [66]. Additionally, Ref. [67] studied quenches in a one-dimensional deformed Ising Hamiltonian (see also [68,69] for related works).

In this work we analyze the transverse field Ising model on a ladder. We find a number of initial product states which feature quasiperiodic revivals in the autocorrelation function, signaling nonthermal behavior. We describe a systematic construction of these states, which in some cases extend from the ladder to higher dimensions. We further provide a number of analytical results, namely an expression for a zero energy transverse field independent eigenstate which we identify as a valence bond solid [70] and which serves as a starting point for a systematic construction of scarred eigenstates [71]. Additional analytical results are obtained for the energy separation between the scarred eigenstates, the degeneracies of the zero transverse field manifolds, and the number of ETH-breaking 'peak' states, which scales as the golden ratio. These results constitute a direct experimental recipe for QMBS in Ising models which have been already realized with Rydberg quantum simulators [72–74] including the ladder geometry [75].

Model. We consider the transverse field Ising model on a $L \times 2$ ladder, with L even, and Hamiltonian

$$H = H_z + H_x = \sum_{\langle i,j \rangle} \sigma_i^z \sigma_j^z + h_x \sum_i \sigma_i^x, \qquad (1)$$

where $\langle i, j \rangle$ denotes nearest neighbors, $\sigma_i^z = c_i^\dagger c_i - c_i c_i^\dagger$, $\sigma_i^x = c_i^\dagger + c_i$ are the Pauli matrices expressed in terms of the hard-core bosonic operators with the usual commutation relations $[c_i, c_j^\dagger] = \delta_{ij}(1 - 2c_i^\dagger c_i)$. We further assume periodic boundary conditions $c_{x+L,y}^\dagger = c_{x,y}^\dagger$, $c_{x,y+2}^\dagger = c_{x,y}^\dagger$ where we have introduced real-space coordinates of each site $i = (x, y)$. The basis states of the Hamiltonian are

$$|b\rangle = \begin{vmatrix} n_{0,1} & n_{1,1} & \dots & n_{L-1,1} \\ n_{0,0} & n_{1,0} & \dots & n_{L-1,0} \end{vmatrix}, \qquad (2)$$

where $n_{x,y} \in \{0, 1\}$ is the occupation number.

---

[*]bavanvoorden@gmail.com
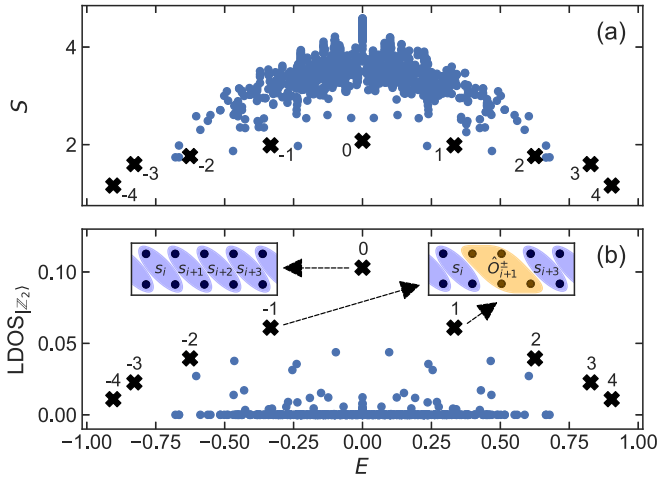[†]minarjiri@gmail.com
[‡]c.j.m.schoutens@uva.nl

FIG. 1. (a) The entanglement entropy and (b) the $\text{LDOS}_{|\mathbb{Z}_2\rangle}$ of the eigenvectors of H', Eq. (3), in the vicinity of $E = 0$ for $L = 8$, $h_x = 0.1$, and $k_x = k_y = 0$. The numbered crosses indicate the $|v_{\text{QMBS},n}\rangle$. The left (right) inset in (b) shows the approximation $|\psi'_{E=0}\rangle$ ($|\psi'_{\text{SMA},\pm1}\rangle$), Eq. (8) [(9)].

For $h_x = 0$ the eigenvectors of H are the states (2) with their energy determined by the difference in the number of equal and unequal neighbor pairs, since each pair $\langle i, j\rangle$ with $n_i = n_j$ ($n_i \neq n_j$) adds $E = 1$ ($E = -1$). This leads to all energy levels being degenerate [76]. The highest (lowest) energy state of $E = 4L$ ($E = -4L$) is reached when all sites have the same $n_{x,y}$ (all neighbors of each site have opposite $n_{x,y}$). Flipping a single spin changes the sign of the energy contribution of all neighboring sites, so that the energy difference between the degenerate manifolds is $|\Delta E| = 4$ with the exception of the lowest (highest) and first (de-)excited ones for which $|\Delta E| = 8$. Defining the potential $V_i \equiv \langle b_i | H_z | b_i\rangle$, the above implies $V_i = 4m_i$ for integer $|m_i| \leqslant L$ [76].

Considering $h_x \neq 0$, we note that $\langle b_i|H_x|b_j\rangle \neq 0$ only if $|b_i\rangle$ and $|b_j\rangle$ differ by a single spin flip. When $V_i \neq V_j$, the perturbative correction to the energies E_i, E_j of this matrix element is of order h_x^2, so that it is strongly suppressed when $h_x \ll 1$. In contrast, basis states with $V_i = V_j$ will hybridize under the perturbation. Consequently, considering a perturbation up to first order in h_x is equivalent to using the projected Hamiltonian

$$H' = H_z + H'_x = \sum_{\langle i,j\rangle} \sigma_i^z\sigma_j^z + h_x\sum_i P\sigma_i^x P, \quad (3)$$

where P acting on $|b_i\rangle$ projects it on all $|b_j\rangle$ with $V_j = V_i$ [77].

Scars. It has been argued that QMBS typically correspond to low entanglement entropy (EE) states [16,26,44]. To this end we consider the (second Rényi) EE $S = -\ln(\text{Tr}(\rho_A^2))$ with ρ_A the density matrix of a subsystem A, which we take to be the half-ladder $L_x = L/2$. The EE spectrum for the $E = 0$ manifold perturbed by the transverse field shows a band of low EE states $|v_{\text{QMBS},n}\rangle$ with $n = -L/2, \ldots, L/2$, characteristic of a QMBS [15], see the crosses in Fig. 1(a).

Additionally, we consider the local density of states of a state $|\psi_0\rangle$,

$$\text{LDOS}_{|\psi_0\rangle}(E) = \sum_j |\langle v_j|\psi_0\rangle|^2 \delta(E - E_j), \quad (4)$$

where $|v_i\rangle$ are the eigenvectors of the Hamiltonian. Using H', it can be seen from Fig. 1(b) that the low EE eigenvectors feature high LDOS for specific product states, namely the $|\mathbb{Z}_2\rangle$ states, a situation analogous to the PXP model. Here $\text{LDOS}_{|\mathbb{Z}_2\rangle}$ is identical for $|\mathbb{Z}_2\rangle$ being

$$|\mathbb{Z}_2^{\text{rung}}\rangle = \begin{vmatrix} 1 & 0 & 1 & 0 & \cdots \\ 1 & 0 & 1 & 0 & \cdots \end{vmatrix}, \quad |\mathbb{Z}_2^{\text{leg}}\rangle = \begin{vmatrix} 1 & 1 & 1 & 1 & \cdots \\ 0 & 0 & 0 & 0 & \cdots \end{vmatrix}$$

$$(5)$$

and their translations $T_x|\mathbb{Z}_2^{\text{rung}}\rangle$ and $T_y|\mathbb{Z}_2^{\text{leg}}\rangle$, where $T_{x,y}$ translates the state by one site in the x, y direction. Denoting by $k_{x,y}$ the eigenvalues of $T_{x,y}$, it is convenient to work in the $k_x = k_y = 0$ momentum sector and therefore we consider either $1/\sqrt{2}(1 + T_x)|\mathbb{Z}_2^{\text{rung}}\rangle$ or $1/\sqrt{2}(1 + T_y)|\mathbb{Z}_2^{\text{leg}}\rangle$.

We note from Fig. 1(b) that the $|v_{\text{QMBS},n}\rangle$ are nondegenerate, except for the one at $E = 0$, and have momentum $k_x = k_y = 0$. Additionally, the energy separations between the special eigenstates are approximately equal. In Fig. 2(a) we show the respective energies $E_{-L/2}, \ldots, E_{L/2}$ and in Fig. 2(b) the differences $\Delta E_j = E_{j+1} - E_j$ between two consecutive energies [78]. As can be seen, the energy differences tend to become more equal for increasing L. A linear fit to ΔE_0 shows that in the limit $L \to \infty$ it becomes $\Delta E_0 \approx 3.49 h_x$.

As a direct consequence of the approximately equal ΔE_j, initializing the system in $|\psi_0\rangle = |\mathbb{Z}_2\rangle$ leads to ETH-breaking behavior. To characterize the ensuing quench dynamics, we consider the autocorrelation [79],

$$A_{|\psi_0\rangle}(t) = |\langle\psi(t)|\psi_0\rangle|^2 = |\langle\psi_0|e^{-iHt}|\psi_0\rangle|^2, \quad (6)$$

which is related to $\text{LDOS}_{|\psi_0\rangle}$ by a Fourier transform [80]. Because of the special properties of $\text{LDOS}_{|\mathbb{Z}_2\rangle}$, the autocorrelation shows revivals of the initial wave function, see Figs. 3(a) and 3(b), where the full Hamiltonian (1) was used with $h_x = 0.1$ and $h_x = 0.7$. Here $A_{|\mathbb{Z}_2\rangle}(t)$ shows revivals, in contrast to the autocorrelation of a typical basis state [76] (for simplicity, here and in the following we omit the explicit normalization unless stated otherwise)

$$|\psi_{\text{typ}}\rangle = \sum_{i=0}^{L-1}\sum_{j=0}^{1} T_x^i T_y^j \begin{vmatrix} 1 & 1 & 1 & 0 & 1 & 1 & 0 & 0 \\ 1 & 0 & 1 & 0 & 1 & 0 & 0 & 0 \end{vmatrix}.$$

$$(7)$$

To compare the response from different initial states, we calculate the average autocorrelation $\langle A\rangle = \lim_{\tau\to\infty}(\tau - t_0)^{-1}\int_{t_0}^{\tau} A(t)\,dt$ [81]. We observe that $\langle A_{|\mathbb{Z}_2\rangle}\rangle$ also remains significantly higher than that of a typical state for h_x beyond the perturbative regime, far from the integrable point at $h_x = 0$, hinting towards the robustness of the ETH breaking in the Ising ladder [76].

Analytical construction of QMBS. We identified an h_x-independent $E = 0$ eigenstate

$$|\psi'_{E=0}\rangle = \prod_i^L s_i|\emptyset\rangle \equiv \prod_i^L (c_{i,1}^\dagger - c_{i+1,0}^\dagger)|\emptyset\rangle, \quad (8)$$

where $|\emptyset\rangle = |{}_0^0 \; \cdots\rangle$ is the vacuum state [76]. $|\psi'_{E=0}\rangle$ is a product state of singlets aligned diagonally in the ladder, see the inset in Fig. 1(b), and thus has valence bond solid (VBS) crystalline order. The knowledge of $|\psi'_{E=0}\rangle$ allows for a
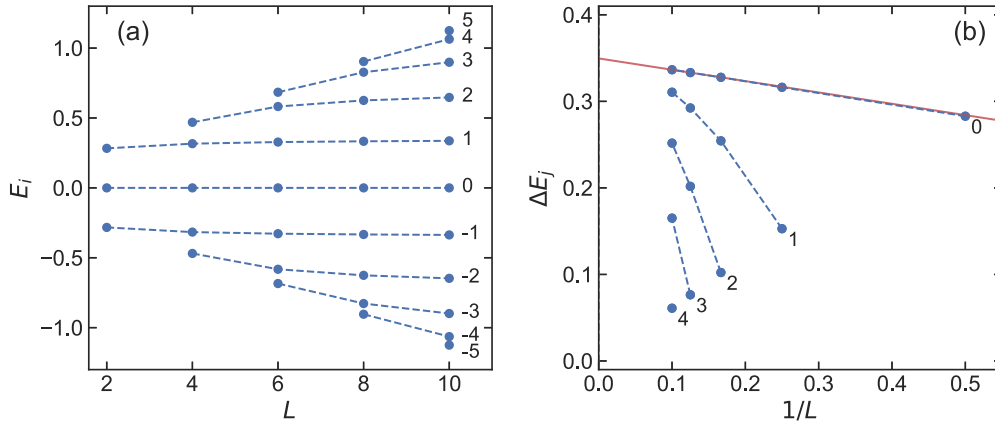
FIG. 2. (a) The energies E_i and (b) energy differences ΔE_j of $\left|v_{\mathrm{QMBS},n}\right\rangle$ as a function of system size for $h_x = 0.1$. The numbering of the states corresponds to Fig. 1. The red line is a linear fit for ΔE_0.

systematic construction of the descendant scarred eigenstates $|v_{\mathrm{QMBS},n}\rangle$. This is achieved by repeated action of a local operator creating quasiparticle excitations on top of $|\psi'_{E=0}\rangle$, a method termed the single mode approximation (SMA) and applied to the PXP model using matrix product states [18]. Motivated by the form of $|\psi'_{E=0}\rangle$, we consider excitations by locally replacing a size 2×2 plaquette with an exact $E_\pm = \pm 2\sqrt{2}h_x$ eigenstate $\hat{O}^\pm|\emptyset\rangle$ of H' (3) with $L = 2$,

$$\hat{O}^\pm = \frac{1}{4}(1 + Q)(c_{0,0}^\dagger + c_{0,1}^\dagger + c_{1,0}^\dagger + c_{1,1}^\dagger)$$
$$\pm \frac{1}{2\sqrt{2}}(c_{0,0}^\dagger c_{0,1}^\dagger + c_{1,0}^\dagger c_{1,1}^\dagger + c_{0,0}^\dagger c_{1,0}^\dagger + c_{0,1}^\dagger c_{1,1}^\dagger), \quad (9)$$

where Q is the particle-hole inversion operator. It has an overlap of $1 - h_x^2/32 + O(h_x^4)$ with the eigenvector of H with $E_\pm = \pm 2\sqrt{2}h_x \mp h_x^3/\sqrt{32} + O(h_x^5)$. However, in order to keep the correct energy, no singlet is allowed to be broken and therefore the excitation operator (9) has to be placed diagonally on the ladder. Consequently, we define the operator $\hat{O}_j^\pm$ as placing an excitation according to Eq. (9) on the sites at $(x, y) = (j, 1)$, $(j + 1, 1)$, $(j + 1, 0)$ and $(j + 2, 0)$, see the
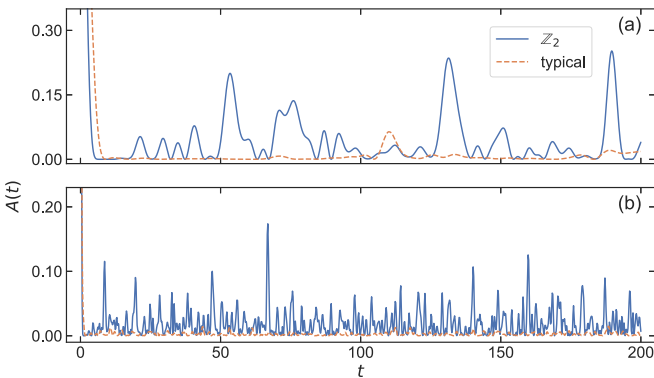

FIG. 3. The autocorrelation Eq. (6) for a $|\mathbb{Z}_2\rangle$ (solid, blue) and a typical (dashed, orange) state for $L = 8$ with (a) $h_x = 0.1$ and (b) $h_x = 0.7$.

inset in Fig. 1(b), such that

$$|\psi'_{\mathrm{SMA},\pm 1}\rangle = \sum_j \hat{O}_j^\pm \prod_{i \neq j, j+1} s_i |\emptyset\rangle. \quad (10)$$

This method can be continued to create approximations to all $|v_{\mathrm{QMBS},n}\rangle$ by adding more local excitations as

$$|\psi'_{\mathrm{SMA},n}\rangle = \sum_{k_1 \ldots k_n} \hat{O}_{k_1}^\pm \ldots \hat{O}_{k_n}^\pm \prod_i s_i |\emptyset\rangle, \quad (11)$$

where the sign in $\hat{O}^\pm$ corresponds to the sign of n, cf. Fig. 1(b). The excitations are not allowed to overlap, so the indices have to obey $i, k_j \neq k_m, k_{m+1} \forall i, j, m$.

The $|v_{\mathrm{QMBS},n}\rangle$ states are symmetric under the reflection of the x coordinates ($R: c_{x,y}^\dagger \to c_{L-x,y}^\dagger$), but the states (8) and (11) are not, because both the singlets and the excitations are diagonal. Therefore we consider the symmetrized states

$$|\psi_{E=0}\rangle = \sqrt{\frac{1}{2 + 2^{3-L}}} (1 + R)|\psi'_{E=0}\rangle \quad (12a)$$

$$|\psi_{\mathrm{SMA,n}}\rangle = \mathcal{N}_n (1 + R)|\psi'_{\mathrm{SMA,n}}\rangle, \quad (12b)$$

where $\mathcal{N}_n$ denotes the n-dependent normalization, e.g., $\mathcal{N}_{\pm 1} = 1/\sqrt{2 + 2^{3-L}L}$ [76]. The state $|\psi_{E=0}\rangle$ is a rather poor approximation to the exact eigenvector, because $|\langle \psi_{E=0}|\mathbb{Z}_2\rangle|^2 = 1/(1 + 2^{L-2})$ is low compared to the special states shown in Fig. 1(b). In contrast, the overlap $|\langle \psi_{\mathrm{SMA,1}}|\mathbb{Z}_2\rangle|^2 = L/(2L + 2^{L-1})$ corresponds well to that in Fig. 1(b) and the fidelity $F_n = |\langle v_{\mathrm{QMBS},n}|\psi_{\mathrm{SMA,n}}\rangle|^2$ with $n = 1$ and $n = 2$, plotted in Fig. 4 for a range of h_x values and $L = 6, 8$, shows that they are a reasonable approximation to the eigenstates. F_n decreases with increasing h_x and L, which is expected due to the h_x-dependent reduced fidelity of the $\hat{O}$ operator to the exact plaquette eigenstates. We note a similar decrease of fidelity also appears in the SMA applied to the PXP model [18]. In the Supplemental Material [76] we present a systematic construction, using the forward scattering approximation (FSA), of a series of states $|w_{(j)}\rangle$, with $|w_{(1)}\rangle = |\psi'_{\mathrm{SMA,1}}\rangle$, converging on an eigenstate $|v'_{\mathrm{QMBS},n}\rangle$ of H', where $|v_{\mathrm{QMBS},n}\rangle = (1 + R)|v'_{\mathrm{QMBS},n}\rangle$.

Regarding the EE, it follows directly from the structure of $|\psi'_{E=0}\rangle$, Eq. (8), that $S_{|\psi'_{E=0}\rangle} = 2\ln(2)$, independent of L and
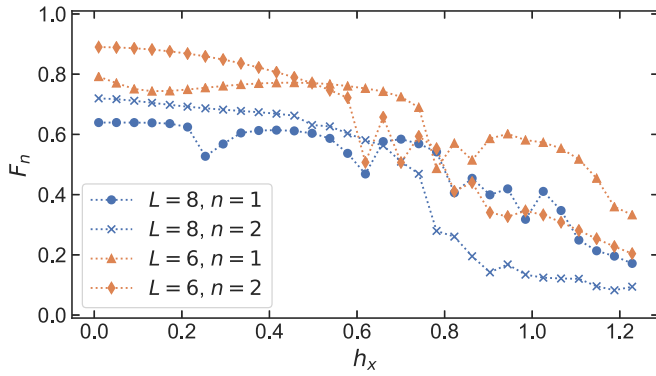
FIG. 4. Fidelity F_n of the first two SMA states vs h_x for $L = 8$ (blue) and $L = 6$ (orange).

of the size of the subsystem, because the two edges of the subsystem always have to cut through one singlet bond each. Furthermore

$$S_{|\psi_{E=0}\rangle} = -\ln\left(\frac{c + w(6 + w)}{8(1 + w)^2}\right), \quad (13)$$

with $w = 2^{L-2}$, and $c = 4$ ($c = 1$) for $L/2$ even (odd) [76]. It reaches its maximum in the thermodynamic limit, $\lim_{L\to\infty} S = 3\ln(2)$ for both $L/2$ odd and even. We thus confirm the expected result, namely that, due to the product state nature of the underlying VBS states, both $|\psi'_{E=0}\rangle$ and $|\psi_{E=0}\rangle$ feature area-law EE in contrast to the typical eigenstates as reflected in Fig. 1(a).

Other ETH-breaking states. In addition to the paradigmatic $|\mathbb{Z}_2\rangle$ states, we were able to identify a family of ETH-breaking product states in the $h_x \ll 1$ limit, which offer a distinct experimental probe. They are characterized by a number of sharp peaks in the LDOS as we now describe.

In the small h_x limit, any connections between basis states with a different potential will be strongly suppressed as $O(h_x^2)$. We can thus identify local spin configurations such that flipping a given spin does not change the potential, which is equivalent to requiring that flipping the spin does not alter the number of (un)equal neighbors (we recall that we use periodic boundary conditions in both directions). This is achieved by configurations of the form

$$\begin{vmatrix} \cdots & n & \underline{n_a} & n & \cdots \\ \cdots & \cdot & 1 - n & \cdot & \cdots \end{vmatrix}, \quad (14)$$

for both $n = 0, 1$. Here, the underline denotes the spin which can be flipped ($n_a \to 1 - n_a$). The $|\mathbb{Z}_2\rangle$ states are special in that every site of them is as in Eq. (14). We will now consider the other extreme, where (almost) no site has this local configuration. Firstly, there are basis states that do not have this pattern anywhere, for example

$$|\psi_p\rangle = \sum_{i,j} T_x^i T_y^j \begin{vmatrix} 1 & 1 & 1 & 1 & 0 & 0 & 1 & 0 \\ 1 & 1 & 1 & 0 & 0 & 0 & 0 & 1 \end{vmatrix}, \quad (15)$$

with $V = 8$. The action of H_x on any site of this basis state will change the potential, so up to first order in h_x the energy is unperturbed and consequently the $\text{LDOS}_{|\psi_p\rangle}$ is sharply peaked around $E = V + O(h_x^2)$ for small values of h_x, see Fig. 5(a). This will be called a peak state. For large L the number of

peak states scales as ϕ^{2L}, where $\phi = (1 + \sqrt{5})/2 \approx 1.618$ is the golden ratio [76].

Secondly, consider a basis state where the configuration (14) only occurs once, such as

$$|\psi_{3p}\rangle = \sum_{i,j} T_x^i T_y^j \begin{vmatrix} 1 & 1 & 1 & 0 & 1 & 1 & 0 & 1 \\ 1 & 1 & 0 & 1 & 1 & 1 & \underline{1} & 1 \end{vmatrix}. \quad (16)$$

Flipping the marked site results in the basis state

$$|\psi_{2p}\rangle = \sum_{i,j} T_x^i T_y^j \begin{vmatrix} 1 & 1 & 1 & 0 & 1 & 1 & \underline{0} & 1 \\ 1 & 1 & 0 & 1 & 1 & 1 & \underline{0} & 1 \end{vmatrix}, \quad (17)$$

which has two sites that could be flipped without a change in the potential. Flipping the lower site returns $|\psi_{2p}\rangle$ to state (16) while flipping the other one leads to

$$|\psi_{3p'}\rangle = \sum_{i,j} T_x^i T_y^j \begin{vmatrix} 1 & 1 & 1 & 0 & 1 & 1 & \underline{1} & 1 \\ 1 & 1 & 0 & 1 & 1 & 1 & 0 & 1 \end{vmatrix}. \quad (18)$$

Here, the energy conserving flip connects again to $|\psi_{2p}\rangle$, such that there is an effective subspace of the states $\{|\psi_{3p}\rangle \leftrightarrow |\psi_{2p}\rangle \leftrightarrow |\psi_{3p'}\rangle\}$ connected by H_x. The eigenvalues are, to leading order in h_x, V and $V \pm \sqrt{2} h_x$, where V is the potential of all three basis states, which in this example is $V = 8$. The eigenvector with energy V has no overlap with the state $|\psi_{2p}\rangle$, resulting in $\text{LDOS}_{|\psi_{2p}\rangle}$ featuring only two peaks at $E = V \pm \sqrt{2} h_x + O(h_x^2)$, see Fig. 5(a). The other two basis states $|\psi_{3p}\rangle$ and $|\psi_{3p'}\rangle$ do have an overlap with the $E = V$ eigenvector and therefore their LDOS consist of three peaks, at $E = V \pm \sqrt{2} h_x + O(h_x^2)$ and $V + O(h_x^2)$. These special overlaps have consequences for the time evolution after a quench from one of these basis states. On one hand, for the single peak the autocorrelation (6) will decay slowly, on a time scale $T \propto 1/O(h_x^2)$ corresponding to the width of the peak. On the other hand, the twin peak state results in a clear oscillation of the autocorrelation with the period given by the energy separation between the two peaks, $T \approx 2\pi/(2\sqrt{2} h_x)$, see Fig. 5(b). When increasing h_x, the peaks in the LDOS will broaden and consequently $\langle A \rangle$ will decrease. In this sense, the
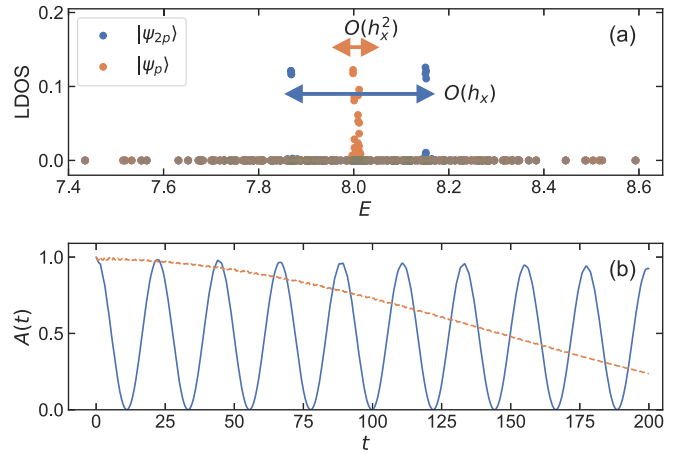

FIG. 5. (a) LDOS and (b) autocorrelation for the single peak state $|\psi_p\rangle$, Eq. (15), (dashed, light, orange), and a twin peaks state $|\psi_{2p}\rangle$, Eq. (17), (solid, dark, blue) with $L = 8$ and $h_x = 0.1$.

ETH-breaking behavior of the peak states is not robust with respect to the increase of h_x, in contrast to the $|\mathbb{Z}_2\rangle$ states.

Importantly, this construction can be generalized to the whole 2D plane, as well as to higher dimensions. As an explicit example, consider the state

$$|\psi_p^{4\times4}\rangle = \left|\begin{matrix} 0 & 1 & 0 & 1 \\ 0 & 0 & 1 & 1 \\ 0 & 1 & 0 & 1 \\ 1 & 1 & 0 & 0 \end{matrix}\right\rangle. \tag{19}$$

We observe that there is no site that is connected to two equal and two unequal neighbors. Therefore flipping any single spin necessarily results in a change of the energy and, in analogy to (15), we conclude that Eq. (19) is a peak state. Next, we note that repeating (19) in x, y directions, such that the system size becomes $4m \times 4n$, $m, n \in \mathbb{N}$, results again in a peak state. This construction can be extended to a hypercubic lattice. One systematic way to accomplish this is by recursively creating the $d + 1$-dimensional lattice by layering $4r$ copies, $r \in \mathbb{N}$, of the d-dimensional lattice, with the seed, when considering $d = 2$, being for example the state $|\psi_p^{4\times4}\rangle$ extended to $4m \times 4n$ sites. Denoting the ith d-dimensional layer as $\mathcal{L}_i$, acting with the particle-hole conjugate operator Q on $\mathcal{L}_i$ when $i \mod 4 = 2$ or $i \mod 4 = 3$ leads to every layer being connected to one layer with all interlayer neighbors equal and one with all interlayer neighbors unequal, such that for every site the total number of equal and unequal neighbors is still different and therefore this is a peak state.

Outlook. In this work we have analyzed transverse field Ising ladder and identified families of initial product states resulting in ETH-violating behavior which can be interpreted as quantum many-body scars. The present analysis allowed us to identify scarred initial states in higher dimensions on a square lattice. This opens a way for generalizations to other geometries, for example the honeycomb lattice featuring frustrated ground states [82]. It would also be interesting to consider the action of the longitudinal field. In one dimension this results in meson excitations [63–66], which are low-variance states [83] akin to the $|\mathbb{Z}_2\rangle$ and peak states, hinting to their relation to many-body scars. The meson quasiparticles are low-energy excitations corresponding to pairwise confined domain walls arising from a doubly degenerate ground state. In contrast, the scar states studied in this work are higher-energy (midspectrum) states which lack a clear interpretation as pairwise confined domain walls. Whether such an interpretation can be found is an interesting open problem. While tackling the outlined questions is theoretically challenging, they can be readily addressed with Rydberg atom based platforms and present thus an ideal testbed for quantum simulations beyond simple chain geometries.

[1] J. M. Deutsch, Phys. Rev. A **43**, 2046 (1991).

[2] M. Srednicki, Phys. Rev. E **50**, 888 (1994).

[3] M. Rigol, V. Dunjko, and M. Olshanii, Nature (London) **452**, 854 (2008).

[4] B. Sutherland, *Beautiful Models: 70 Years of Exactly Solved Quantum Many-Body Problems* (World Scientific Publishing Company, River Edge, NJ, 2004).

[5] M. Takahashi, *Thermodynamics of One-Dimensional Solvable Models* (Cambridge University Press, Cambridge, 2005).

[6] I. V. Gornyi, A. D. Mirlin, and D. G. Polyakov, Phys. Rev. Lett. **95**, 206603 (2005).

[7] D. M. Basko, I. L. Aleiner, and B. L. Altshuler, Ann. Phys. **321**, 1126 (2006).

[8] M. Serbyn, Z. Papić, and D. A. Abanin, Phys. Rev. Lett. **111**, 127201 (2013).

[9] D. A. Huse, R. Nandkishore, and V. Oganesyan, Phys. Rev. B **90**, 174202 (2014).

[10] R. Nandkishore and D. A. Huse, Annu. Rev. Condens. Matter Phys. **6**, 15 (2015).

[11] J. Z. Imbrie, J. Stat. Phys. **163**, 998 (2016).

[12] J. Z. Imbrie, V. Ros, and A. Scardicchio, Ann. Phys. **529**, 1600278 (2017).

[13] H. Bernien, M. D. Lukin, H. Pichler, S. Choi, M. Greiner, V. Vuletić, A. Omran, H. Levine, S. Schwartz, A. Keesling, M. Endres, and A. S. Zibrov, Nature (London) **551**, 579 (2017).

[14] I. Lesanovsky and H. Katsura, Phys. Rev. A **86**, 041601(R) (2012).

[15] C. J. Turner, A. A. Michailidis, D. A. Abanin, M. Serbyn, and Z. Papić, Phys. Rev. B **98**, 155134 (2018).

[16] C. J. Turner, A. A. Michailidis, D. A. Abanin, M. Serbyn, and Z. Papić, Nat. Phys. **14**, 745 (2018).

[17] S. Choi, C. J. Turner, H. Pichler, W. W. Ho, A. A. Michailidis, Z. Papić, M. Serbyn, M. D. Lukin, and D. A. Abanin, Phys. Rev. Lett. **122**, 220603 (2019).

[18] C.-J. Lin and O. I. Motrunich, Phys. Rev. Lett. **122**, 173401 (2019).

[19] T. Iadecola, M. Schecter, and S. Xu, Phys. Rev. B **100**, 184312 (2019).

[20] F. M. Surace, P. P. Mazza, G. Giudici, A. Lerose, A. Gambassi, and M. Dalmonte, Phys. Rev. X **10**, 021041 (2020).

[21] C.-J. Lin, A. Chandran, and O. I. Motrunich, arXiv:1910.07669.

[22] K. Bull, J.-Y. Desaules, and Z. Papić, Phys. Rev. B **101**, 165139 (2020).

[23] D. K. Mark, C.-J. Lin, and O. I. Motrunich, Phys. Rev. B **101**, 094308 (2020).

[24] C.-J. Lin, V. Calvera, and T. H. Hsieh, arXiv:2003.04516.

[25] Y. Yang, S. Iblisdir, J. I. Cirac, and M. C. Bañuls, Phys. Rev. Lett. **124**, 100602 (2020).

[26] W. W. Ho, S. Choi, H. Pichler, and M. D. Lukin, Phys. Rev. Lett. **122**, 040603 (2019).

[27] K. Bull, I. Martin, and Z. Papić, Phys. Rev. Lett. **123**, 030601 (2019).

[28] N. Pancotti, G. Giudice, J. I. Cirac, J. P. Garrahan, and M. C. Bañuls, Phys. Rev. X **10**, 021051 (2020).

[29] S. Roy and A. Lazarides, Phys. Rev. Research **2**, 023159 (2020).

[30] S. Ok, K. Choo, C. Mudry, C. Castelnovo, C. Chamon, and T. Neupert, Phys. Rev. Research **1**, 033144 (2019).

[31] V. Khemani, C. R. Laumann, and A. Chandran, Phys. Rev. B **99**, 161101(R) (2019).

[32] A. Hallam, J. Morley, and A. G. Green, Nat. Commun. **10**, 1 (2019).

[33] D. Jansen, J. Stolpp, L. Vidmar, and F. Heidrich-Meisner, Phys. Rev. B **99**, 155130 (2019).

[34] S. Moudgalya, T. Devakul, C. W. von Keyserlingk, and S. L. Sondhi, Phys. Rev. B **99**, 094312 (2019).

[35] H. Wilming, M. Goihl, I. Roth, and J. Eisert, Phys. Rev. Lett. **123**, 200604 (2019).

[36] A. A. Michailidis, C. J. Turner, Z. Papić, D. A. Abanin, and M. Serbyn, Phys. Rev. X **10**, 011055 (2020).

[37] A. Andreev, A. Balanov, T. Fromhold, M. Greenaway, A. Hramov, W. Li, V. Makarov, and A. Zagoskin, arXiv:1907.03602.

[38] Y. Werman, arXiv:2001.06110.

[39] G. De Tomasi, D. Hetterich, P. Sala, and F. Pollmann, Phys. Rev. B **100**, 214313 (2019).

[40] V. Khemani and R. Nandkishore, Phys. Rev. B **101**, 174204 (2020).

[41] P. Sala, T. Rakovszky, R. Verresen, M. Knap, and F. Pollmann, Phys. Rev. X **10**, 011047 (2020).

[42] P. Karpov, R. Verdel, Y.-P. Huang, M. Schmitt, and M. Heyl, arXiv:2003.04901.

[43] S. Moudgalya, S. Rachel, B. A. Bernevig, and N. Regnault, Phys. Rev. B **98**, 235155 (2018).

[44] S. Moudgalya, N. Regnault, and B. A. Bernevig, Phys. Rev. B **98**, 235156 (2018).

[45] N. Shiraishi, J. Stat. Mech. (2019) 083103.

[46] D. K. Mark, C.-J. Lin, and O. I. Motrunich, Phys. Rev. B **101**, 195131 (2020).

[47] S. Moudgalya, E. O'Brien, B. A. Bernevig, P. Fendley, and N. Regnault, arXiv:2002.11725.

[48] S. Chattopadhyay, H. Pichler, M. D. Lukin, and W. W. Ho, Phys. Rev. B **101**, 174308 (2020).

[49] M. Schecter and T. Iadecola, Phys. Rev. Lett. **123**, 147201 (2019).

[50] T. Iadecola and M. Žnidarič, Phys. Rev. Lett. **123**, 036403 (2019).

[51] N. Shibata, N. Yoshioka, and H. Katsura, Phys. Rev. Lett. **124**, 180604 (2020).

[52] K. Lee, R. Melendrez, A. Pal, and H. J. Changlani, arXiv:2002.08970.

[53] Y. Chen and Z. Cai, Phys. Rev. A **101**, 023611 (2020).

[54] S. Sinha and S. Sinha, arXiv:1912.06593.

[55] D. Villaseñor, S. Pilatowsky-Cameo, M. A. Bastarrachea-Magnani, S. Lerma, L. F. Santos, and J. G. Hirsch, New J. Phys. (2020), doi:10.1088/1367-2630/ab8ef8.

[56] S. Pai and M. Pretko, Phys. Rev. Lett. **123**, 136401 (2019).

[57] A. Pizzi, J. Knolle, and A. Nunnenkamp, arXiv:1910.07539.

[58] S. Sugiura, T. Kuwahara, and K. Saito, arXiv:1911.06092.

[59] H. Zhao, J. Vovrosh, F. Mintert, and J. Knolle, Phys. Rev. Lett. **124**, 160604 (2020).

[60] B. Mukherjee, A. Sen, D. Sen, and K. Sengupta, arXiv:2002.08683.

[61] H. H. Jen, Phys. Rev. Research **2**, 013097 (2020).

[62] C.-h. Fan, D. Rossini, H.-X. Zhang, J.-H. Wu, M. Artoni, and G. C. La Rocca, Phys. Rev. A **101**, 013417 (2020).

[63] A. J. A. James, R. M. Konik, and N. J. Robinson, Phys. Rev. Lett. **122**, 130603 (2019).

[64] N. J. Robinson, A. J. A. James, and R. M. Konik, Phys. Rev. B **99**, 195108 (2019).

[65] F. Liu, R. Lundgren, P. Titum, G. Pagano, J. Zhang, C. Monroe, and A. V. Gorshkov, Phys. Rev. Lett. **122**, 150601 (2019).

[66] M. Kormos, M. Collura, G. Takács, and P. Calabrese, Nat. Phys. **13**, 246 (2017).

[67] T. Iadecola and M. Schecter, Phys. Rev. B **101**, 024306 (2020).

[68] A. Bukva, P. Sabella-Garnier, and K. Schalm, arXiv:1911.06292.

[69] G. Magnifico, M. Dalmonte, P. Facchi, S. Pascazio, F. Pepe, and E. Ercolessi, Quantum **4**, 281 (2020).

[70] I. Affleck, T. Kennedy, E. H. Lieb, and H. Tasaki, Phys. Rev. Lett. **59**, 799 (1987).

[71] Recently, we became aware of Ref. [24] which has identified QMBS in the two-dimensional PXP model linking them also to the VBS.

[72] P. Schauß, J. Zeiher, T. Fukuhara, S. Hild, M. Cheneau, T. Macrì, T. Pohl, I. Bloch, and C. Groß, Science **347**, 1455 (2015).

[73] H. Labuhn, D. Barredo, S. Ravets, S. De Léséleuc, T. Macrì, T. Lahaye, and A. Browaeys, Nature (London) **534**, 667 (2016).

[74] A. Browaeys and T. Lahaye, Nat. Phys. **16**, 132 (2020).

[75] S. de Léséleuc, V. Lienhard, P. Scholl, D. Barredo, S. Weber, N. Lang, H. P. Büchler, T. Lahaye, and A. Browaeys, Science **365**, 775 (2019).

[76] See Supplemental Material at http://link.aps.org/supplemental/10.1103/PhysRevB.101.220305 for (i) the counting of the degeneracies of the H_z eigenstates, (ii) details on the evaluation of the autocorrelation function, (iii) the derivation of the $|\psi'_{E=0}\rangle$ state, (iv) the FSA construction, (v) derivation of the EE, and (vi) counting of the peak states [84–87].

[77] Despite the similarity, the Hamiltonian H' is not equal to the PXP model due to the difference in the projection operators P.

[78] We note that $\Delta E_{-j} = \Delta E_{j-1}$ for $j > 0$ due to the spectral inversion symmetry.

[79] Á. M. Alhambra, A. Anshu, and H. Wilming, Phys. Rev. B **101**, 205107 (2020).

[80] E. J. Heller, Phys. Rev. Lett. **53**, 1515 (1984).

[81] We take $t_0 > 0$ such that the initial decay of $A(t)$ is not included in the average and τ big enough such that $\langle A \rangle$ is τ independent [76].

[82] T. Coletta, J.-D. Picon, S. E. Korshunov, and F. Mila, Phys. Rev. B **83**, 054402 (2011).

[83] Neil J. Robinson (private communication).

[84] To this end we note that for initial product states considered in this work, the time dependent autocorrelation constitutes a directly accessible experimental probe. This can be achieved by projecting on individual basis states as described, e.g., in Ref. [13].

[85] P. Mazur, Physica **43**, 533 (1969).

[86] M. Suzuki, Physica **51**, 277 (1971).

[87] J.-S. Caux and J. Mossel, J. Stat. Phys. (2011) P02023.